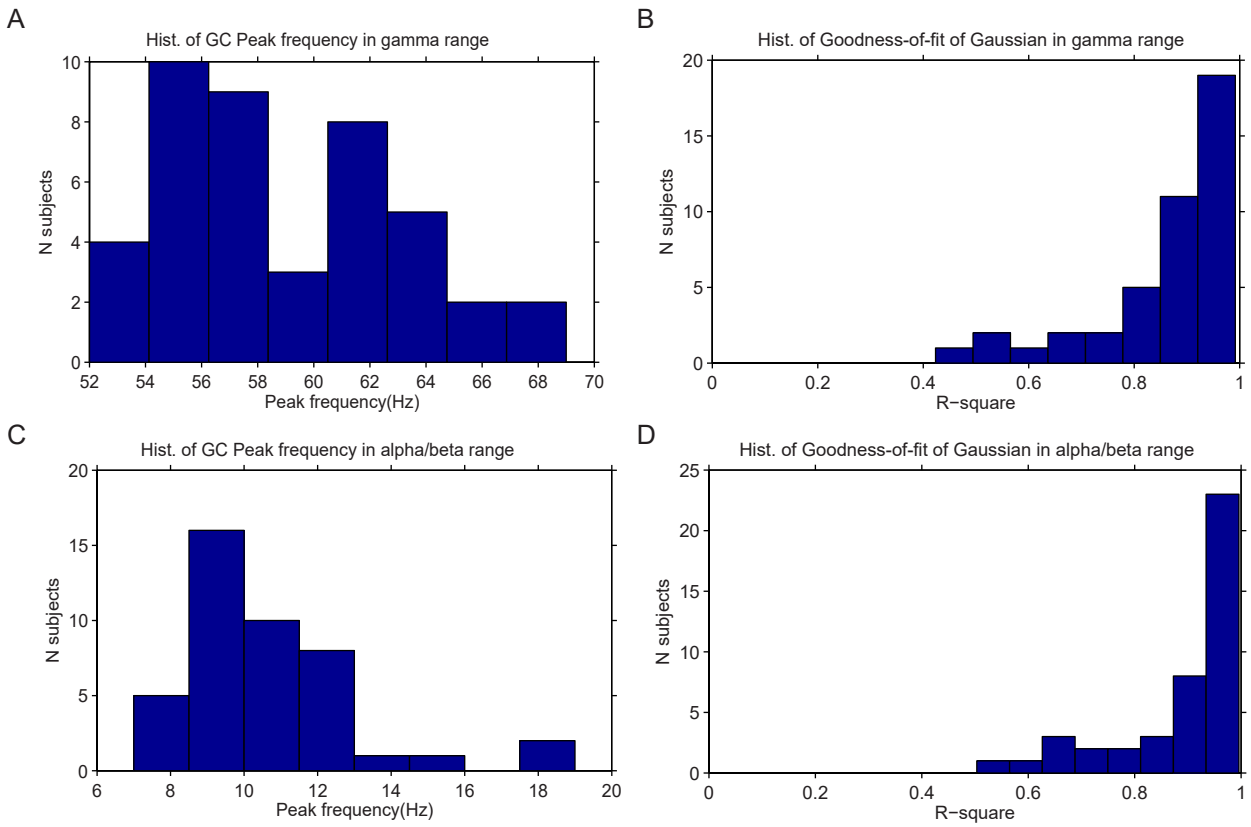

Supplemental Figure 1

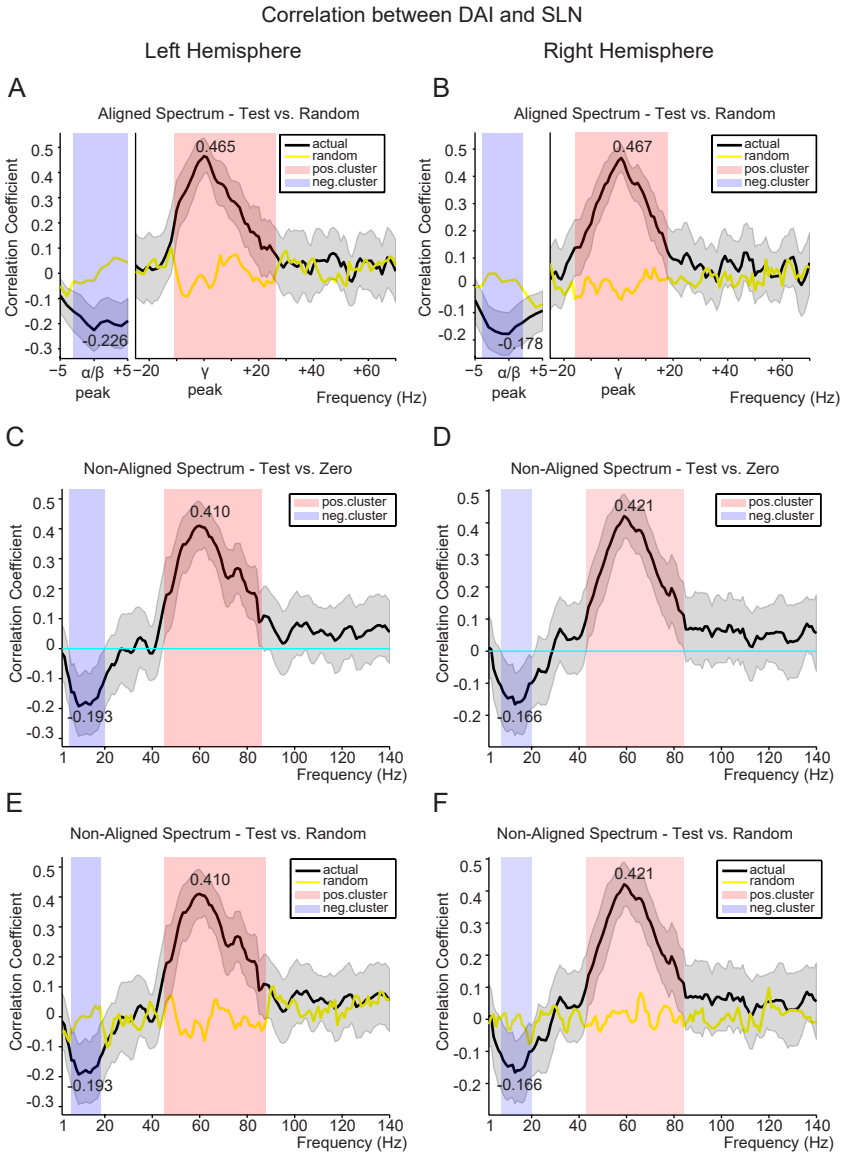

Supplemental Figure 2

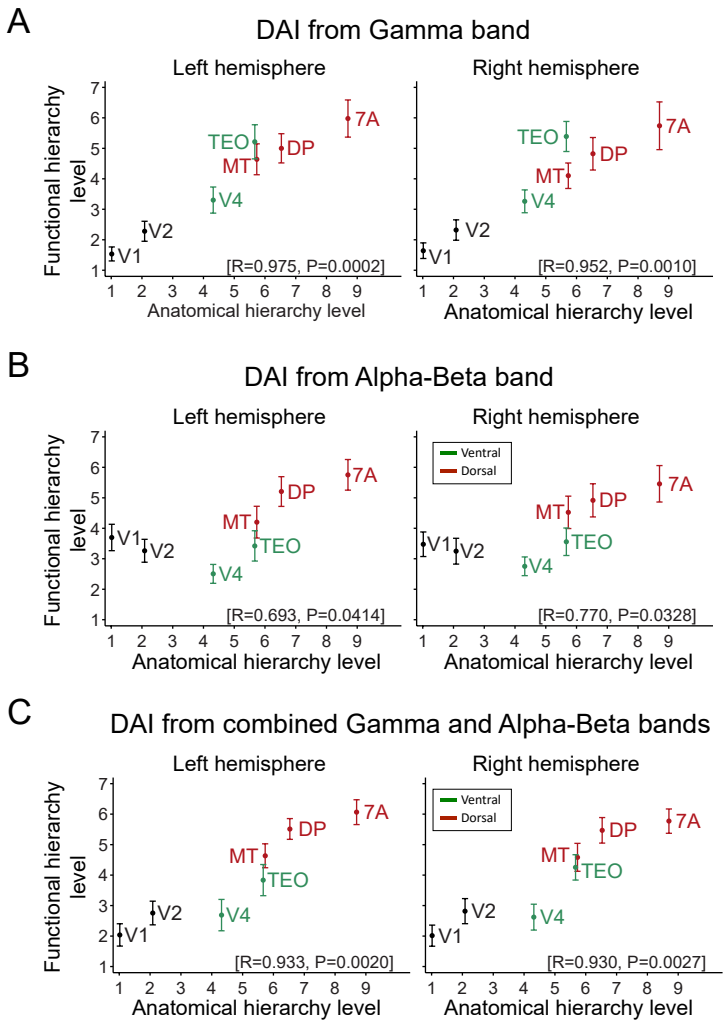

Supplemental Figure 3

Area Name	N dipoles in Left Hemisphere	N dipoles in Right Hemisphere
V1	31	28
V2	40	38
V3	49	44
V3A	9	10
V3B	12	8
V3C	11	11
V3D	8	8
V4	9	10
V4t	2	3
LO1	14	15
LO2	11	9
PITd	3	2
PITv	3	2
MT	3	8
VO1	11	7
MST	2	2
FST	2	2
ER	22	22
V7	5	6
IPS1	5	5
IPS2	6	6
IPS3	15	15
IPS4	12	12
7A	56	58
FEF	24	20

Supplemental Table 1

Supplemental Data

Figure S1, related to Figure 5. Distributions of individual peak frequencies in Gamma and Alpha-Beta bands

For each subject, Gaussian functions were fit to the GC spectrum averaged over all area pairs of both hemispheres, separately for the frequency ranges 4-20 Hz (A, C) and 30-100 Hz (B, D). (A) Histogram of peak frequencies across the 43 subjects in the 4-20 Hz range. (B) Histogram of goodness-of-fit measure (r-square) of the Gaussian function in the 4-20 Hz range across the 43 subjects. (C) Same as (A), but for 30-100 Hz range. (D) Same as (B), but for 30-100 Hz range. Notice that the goodness-of-fit distribution is heavily skewed towards 1, indicating good fitting results.

Figure S2, related to Figure 6. DAI-SLN correlation spectra versus randomized surrogate data and without peak-frequency alignment.

In order to test whether there was any bias in the DAI-SLN correlation presented in Fig. 6, epochs were shuffled prior to computing GC and the subsequent DAI-SLN correlation. In (A) and (B), for left and right hemispheres respectively, this randomized surrogate correlation is depicted by the yellow line. Significance was again assessed with the same non-parametric permutation based tests. Very similar positive and negative frequency clusters were found in the gamma and alpha-beta ranges respectively. (C,D) DAI-SLN correlation spectra without peak-frequency alignment. For these analyses, the spectrum of each subject has not been aligned relative to the individual peaks in the gamma and alpha-beta bands, as was done in Figure 6. Rather the DAI-SLN correlation spectra are averaged over subjects without alignment. Significance is assessed relative to zero correlation as in Fig. 6. (E,F) DAI-SLN correlation without peak-frequency alignment as in (C,D), and testing against random correlation as in (A, B). Note that without peak-frequency alignment, peak correlation values are slightly lower.

Figure S3, related to Figure 7. Granger-Causality-based hierarchy versus anatomical hierarchy without peak-frequency alignment.

This figure presents the relation of the human functional hierarchy derived for DAI values versus the macaque anatomical hierarchy from SLN values, similar to Figure 7, but without alignment of individual peak frequencies. In the same fashion as in Figure 7, three cases were investigated, namely with the functional hierarchy computed from (A) DAI in the gamma band, (B) DAI in the alpha-beta band and (C) the combined DAI in alpha-beta and gamma bands. Early visual areas are depicted in black, ventral-stream areas in green, and dorsal-stream areas in red. Inset brackets on bottom right of each subplot report Pearson correlation between human functional and macaque anatomical hierarchical levels. Results were qualitatively the same as in Fig. 7.

Table S1, related to Figure 2. Number of dipoles within each of the 26 visual areas in the left and right hemispheres of the MEG source model.

Supplemental Experimental Procedures

Data Acquisition

MEG: Recordings were performed with a whole-head MEG system (CTF Systems Inc.) comprising 275 axial gradiometers, located at the Donders Institute of Radboud University Nijmegen (Nijmegen, Netherlands). In addition, horizontal and vertical Electrooculograms (EOG) were recorded using bipolar electrodes for off-line eye-movement artifact rejection. All signals were low-pass filtered at 300 Hz, sampled at 1200 Hz, and stored. Head position relative to the gradiometer array was determined prior and after the MEG recording using 3 coils attached to subject's nasion, left and right ear canals.

MRI: Structural MR images were acquired using an Avanto 1.5 T whole body MRI scanner (Siemens, Germany). A volume head coil was used for RF transmission and signal reception. The scan was performed with a 3D MPRAGE sequence with 1 mm isotropic resolution.

Subjects

Datasets of 43 subjects were selected from a pool of 160 subjects, which had been recorded for genotyping of parameters derived from visually induced gamma-band activity. The genotyping study required a large number of subjects and was fully focused on gamma, and it therefore accepted subjects, in which sub-gamma activity was confounded by artifacts. For the present study, subjects were excluded if 1) their body carried ferromagnetic elements causing low-frequency MEG artifacts (e.g. metallic orthodontic retainers), 2) they did not have normal vision, 3) they used medication, 4) they exhibited head movements larger than 10 mm during the experiment. This left 43 subjects (36 right-handed) with an average age of 23.1 (range: 18 to 34). All subjects gave written informed consent according to guidelines of the local ethics committee (Commissie Mensgebonden Onderzoek Regio Arnhem-Nijmegen, The Netherlands).

Human Brain Model

For source analysis, structural MR images were acquired for each individual subject, and the cortical mantle was extracted with the FreeSurfer longitudinal stream pipeline (Reuter et al., 2012). Cortical parcellation and area definition used a recent visuotopic atlas provided by (Abdollahi et al., 2014), the FreeSurfer software suite (http://FreeSurfer.net/) (Fischl et al., 2004; Desikan et al., 2006; Destrieux et al., 2010) and the Caret software suite (http://brainvis.wustl.edu/) (Glasser and Van Essen, 2011; Van Essen et al., 2012).

The cortical sheet extracted from FreeSurfer was transformed and registered into the Caret representation through the Caret pipeline "freesurfer_to_fs_LR". In Caret, the Conte69 atlas is defined and contains a composite parcellation (Van Essen et al., 2012) which includes multiple visuotopic areas in the occipital, parietal and temporal lobe, which have been mapped based on a number of studies. The recent visuotopic atlas provided by (Abdollahi et al., 2014) is based on Maximum Probability Maps (MPMs) for 18 human visual areas, that have been built based on recent Multimodal Surface Matching (MSM) algorithms for inter-subject registration, which utilize as registration features not only structural cortical characteristics but also retinotopic activation maps. The resulting parcellation provides a more refined cortical representation of these 18 cortical areas as compared to previous studies. This parcellation atlas is represented on the fs_LR cortical surface template, similarly to the

Conte69 visuotopic atlas. Hereafter, for convenience, this parcellation will be referred to in this text as the "Abdollahi2014" parcellation. Finally, one of the parcellation schemes of FreeSurfer, "aparc.a2009s" (Destrieux et al., 2010), provides parcels segregating all the main gyri and sulci of the human cortex and was used in addition to the visuotopic Conte69 and the parcellations from Caret, as explained in more detail below.

Both, the FreeSurfer and Caret cortical sheet representations contain more than 10^5 vertices per hemisphere and were subsampled for MEG source analysis with the MNE software suite (Gramfort et al., 2014). Through recursive icosahedron subdivision, this software subsamples the dense FreeSurfer cortical representation by a fixed number of 4098 vertices per hemisphere. Those vertices were mapped to their nearest neighbors in the Caret common template surface representation and thereby to the Conte69 atlas. The vertex positions were then transformed into the head coordinate system, where the MEG measurements were acquired and the inverse solution was computed.

Selection of 7 homologous brain areas between human and macaque

V1, V2: In both macaque and human brains, V1 and V2 are the largest cortical areas and have the clearest homology between these species (Van Essen, 2005). They are both available in the Abdollahi2014 atlas labelled as V1 and V2 respectively.

MT: In the macaque, area MT is located on the posterior bank of the superior temporal sulcus, is characterized by its distinct heavy myelination, and contains a complete topographic representation of the contralateral visual field (Van Essen et al., 1981). In the human brain, area MT has been consistently mapped at a corresponding location, has a similar visuotopic organization and is characterized by its motion-selective activation (Huk et al., 2002; Fischl et al., 2008; Kolster et al., 2010). The area used here is area MT/V5 in the so called MT/V5+ complex identified in the human brain (Kolster et al., 2010). This area is available in the Abdollahi2014 atlas, labelled as MT.

V4 (hV4): In the macaque, area V4 has been mapped both physiologically and with functional MRI. It consists of 2 parts, a dorsal lower field representation and a ventral upper-field representation. The horizontal meridian is represented anterior to both ventral and dorsal V4 in the macaque brain (Fize et al., 2003; Janssens et al., 2014; Kolster et al., 2014). In the human brain the strongest evidence of homology comes mainly from the ventral part of human V4, which has been mapped by various studies in a corresponding location and with similar visuotopic organization (Brewer et al., 2005; Van Essen, 2005; Swisher et al., 2007; Kolster et al., 2010). This area is available in the Abdollahi2014 atlas, labelled as hV4.

DP (V7): In the macaque brain, visual area DP occupies the dorsal aspect of the prelunate gyrus immediately anterior to area V3A. In the human brain, an area located also just anteriorly to area V3A (as defined in (Tootell et al., 1998) or V3D as defined in (Georgieva et al., 2009) and (Abdollahi et al., 2014)) with a putative homology in its retinotopic representation has been identified by (Tootell et al., 1998) and given the name V7. This area is available in the Abdollahi2014 atlas, labelled as V7.

TEO (PIT): In the macaque brain, according to (Felleman and Essen, 1991), the posterior part of the inferotemporal cortex is divided into two regions labelled as PITd (dorsal) and PITv (ventral). These areas coincide largely with the architectonic Temporal Occipital area (TEO). In the human brain, the putative homologous areas have been mapped using functional MRI, have been shown to be involved in processing two-dimensional shape, and they have been given the same names as in the macaque

(Kolster et al., 2010). These areas are available in the Abdollahi2014 atlas labelled as phPITd and phPITv. Here, these ventral and dorsal parcels have been collapsed into a single parcel called PIT.

7A (Gyrus parietalis inferior – Angular gyrus): In the macaque brain, area 7A occupies the caudal part of the Inferior Parietal Lobule (IPL) and extends only a short distance into the intraparietal sulcus (Felleman and Essen, 1991). In an alternative, widely used parcellation scheme of the macaque IPL by (Pandya and Seltzer, 1982) this area was attributed to 2 areas of the caudal IPL, namely the areas labelled as PG and Opt. In the human brain, (Caspers et al., 2011) identified 2 homologous areas through diffusion-weighted MRI, spanning the caudal part of human IPL and showing strong resemblance in their connectivity patterns with that of the macaque. In the human visuotopic parcellation scheme available in the Conte69 atlas, no parcel covers the caudal part of IPL, where this homology has been identified. In FreeSurfer's "aparc.a2009s" parcellation scheme (Destrieux et al., 2010) the caudal IPL is covered by the parcel labelled as "G_pariet_inf-Angular", which primarily encapsulates the angular gyrus and is segregated from rostral IPL by the sulcus intermedius premus. Dorsally it extends into the intrapariatal sulcus (IPS). Based on the above anatomical characteristics, this parcel was selected as homologous to macaque area 7A.

As mentioned above, the dense cortical surface representation of the common template "fs_LR" surface was down-sampled for the MEG source analysis. Accordingly, the representation of the selected areas was defined in this subsampled space.

Details on the Selection of 26 visual areas from the human brain

V1, V2, V4, MT, V7, 7A: These areas are the same that were used in the 7-area analysis (see above and Experimental Procedures).FEF: The Frontal Eye Field is a cortical area located in humans around the intersection of the pre-central sulcus with the dorsal portion of the superior frontal sulcus. It is considered a "hub", having anatomical connections with visual, parietal, temporal and prefrontal areas. Functionally it is involved in oculomotor behavior, visuo-spatial attention, visual awareness and perceptual modulation (Vernet et al., 2014). In the visuotopic parcellation of the Conte69 atlas, an FEF parcel is not available. The most relevant parcel that is available is Brodmann area 8, in which FEF occupies only a relatively small portion. In order to represent FEF, only the ventral branch of the superior precentral sulcus and its intersection with the superior frontal sulcus were manually selected as the parcel that represents FEF (Amiez and Petrides, 2009).

The following areas are available in the atlas dataset of (Abdollahi et al., 2014) which in the following text will be referred to as "Abdollahi2014":

V3: Area V3, in both human and monkey, consists of a lower and an upper field representation, neighboring area V2 dorsally and ventrally respectively. Although these dorsal and ventral parts have been shown to have some asymmetries in their function, architecture and connectivity, they are considered in both human and monkey as the constituents of a single retinotopic area (Van Essen, 2005).

V3A, V3B, V3C, V3D: These areas that span the cortical surface adjoined dorsally to area V3 were identified by (Georgieva et al., 2009). Therein, they are jointly referred to as the "V3A complex" and they represent the same cortical areas previously referred to as V3A and V3B (Wandell et al., 2007). The dorsal areas of the complex, V3C and V3D, adjoin ventrally area V7. These areas contain neurons with larger retinotopic fields than areas V1, V2 and V3. These areas have been implicated in motion processing, with areas V3A and V3B (corresponding to area V3B in (Fischer, 2011)) having a higher

preference for externally induced retinal motion, and areas V3C and V3D (corresponding to area V3A in (Fischer, 2011)) having a higher preference for real motion.

LO1, LO2: Lateral Occipital Areas 1 and 2. These areas are located in the fundus of the lateral occipital sulcus between dorsal V3 and MT, with LO2 anterior to LO1. The retinotopy of these areas is less precise and more variable than early visual areas. It has been suggested that these two areas represent shape information, with LO1 extracting boundary information and LO2 extracting regions and representing shape (Larsson and Heeger, 2006; Wandell et al., 2007).

PITv, PITd: These two areas are the constituents of area PIT used in the 7-area analysis. In the 26-area analysis PIT is replaced by these two areas.

MT, pMSTv, pFST, pV4t: These four areas comprise the human middle temporal MT/V5+ complex, homologous to the MT/V5 complex in the monkey brain. This complex consists of the middle temporal area (MT/V5), the putative ventral part of the medial superior temporal area (pMSTv), the putative fundus of the superior temporal area (pFST) and the putative V4 transitional zone. Area V4t is adjoined ventrally to MT/V5 and dorsally to phPITd. Area pMSTv is located rostrally to area MT/V5. Area pFST is located anteriorly to area V4t and ventrally to area pMSTv. All four areas respond strongly to motion, have much larger receptive fields than V1 and are considered parts of the dorsal stream. Within the MT/V5+ complex, area pMSTv has the largest receptive fields. The more ventral areas of the complex, V4t and pFST, respond stronger to shapes, while the more dorsal areas, MT/V5 and pMSTv respond stronger to 3D structure from motion (Kolster et al., 2010). Area MT here is the same as the one used in the 7-area analysis.

VO1: Area VO1 is part of Ventral Occipital areas(VO) located on the fusiform gyrus anteriorly of area hV4 and is considered part of the ventral stream. It has a preference for foveal and parafoveal eccentricities. Due to the fact that VO areas show little object selectivity, it has been hypothesized that they play an intermediate visual processing role between early visual cortex and higher order object-selective cortex (Brewer et al., 2005; Arcaro et al., 2009; Kolster et al., 2010).

The following areas are available in the visuotopic parcellation of the Conte69 atlas:

IPS1, IPS2, IPS3, IPS4: These four parcels are subdivisions of the posterior medial bank of the intra-pariatel sulcus(IPS) with distinct retinotopic maps, numbered from posterior to anterior locations. Numerous functions related to visual processing such as visual attention, saccadic preparation and multisensory integration have been shown to activate these areas (Swisher et al., 2007).

ER: The entorhinal cortex, located in the medial temporal lobe, comprises of a set of cortical areas that are known to be a major gateway to and from the hippocampus. Based on its anatomical connectivity and functional properties, it has been categorized as multimodal association cortex. Although it is not retinotopically organized, it has strong connections with some visual areas (Felleman and Essen, 1991) and it has recently been shown to play an important role in spatial navigation (Moser et al., 2008).

Area 46: Brodmann area 46 corresponds with the dorsolateral prefrontal cortex in and around the middle third of the principal sulcus. It has strong connections mainly with parietal and temporal cortex (Petrides and Pandya, 1999). There has been strong evidence that functionally it is involved in maintaining and manipulating information in working memory (Krawczyk, 2002).

Retrograde tracing database

Description of the anatomical dataset acquisition and analysis has been reported in (Markov et al., 2014). The values that we used correspond to multiple injections each into V1, V2, V4 and single injections into areas MT, DP, TEO and 7A. Only SLN values based on at least 10 labeled neurons were included. Three projections had fewer than 10 neurons labeled, and their SLN was therefore considered unreliably quantified. These projections were V1-to-DP, V1-to-7A and V2-to-7A. The V1-to-TEO projection was reported as missing i.e. no labeled neurons found in V1 after TEO injection. For these projections, there is strong evidence in the literature that they are present and all have a feedforward characteristic, and this was used in place of SLN evidence. Updates, atlases and additional information concerning the anatomical dataset that was used for this work is available at www.core-nets.org.

Inverse solution

Subject-wise structural MRI scans were used to derive individual single-shell volume conductor models (Nolte, 2003). The inverse solution was then performed using Linearly Constrained Minimum Variance (LCMV) adaptive spatial filtering, often referred to as “Beamforming” (Van Veen et al., 1997). The beamformer gives, for each of a set of predefined locations, a coefficient matrix such that the multiplication of the matrix with the sensor-level signals provides an estimate of the dipole moment at that location, while minimizing influences of other, linearly uncorrelated sources. We used this approach to scan a set of dipole locations on the cortical mesh. As the beamformer output is simply a linear projection of sensor-level data, it does not only apply to the raw signal of the different MEG sensors but also to any linear decomposition, like the Fourier transform of the raw signal.

There are beamformer methods that derive spatial filters for each frequency separately (Gross et al., 2001). They are mostly suited to provide source estimates for selected frequency bands. The current work investigates the entire spectrum, and focuses on GC, whose estimation entails multiple neighboring frequencies. Therefore, we opted to estimate the source spectrum by means of the LCMV broadband inverse solution. The LCMV solution is based on the broadband covariance matrix of the non-averaged MEG sensor data. When determining the LCMV solution, we used a regularization parameter of 20% of the covariance matrix.

The set of brain locations for which the inverse solution was computed comprised of all the points distributed within the human visual cortical areas of interest in each hemisphere.

Supplemental References

Abdollahi RO, Kolster H, Glasser MF, Robinson EC, Coalson TS, Dierker D, Jenkinson M, Van Essen DC, Orban GA (2014) Correspondences between retinotopic areas and myelin maps in human visual cortex. Neuroimage 99:509-524.

Amiez C, Petrides M (2009) Anatomical organization of the eye fields in the human and non-human primate frontal cortex. Prog Neurobiol 89:220-230.

Arcaro MJ, McMains SA, Singer BD, Kastner S (2009) Retinotopic organization of human ventral visual cortex. J Neurosci 29:10638-10652.

Brewer AA, Liu J, Wade AR, Wandell BA (2005) Visual field maps and stimulus selectivity in human ventral occipital cortex. Nat Neurosci 8:1102-1109.

Caspers S, Eickhoff SB, Rick T, von Kapri A, Kuhlen T, Huang R, Shah NJ, Zilles K (2011) Probabilistic fibre tract analysis of cytoarchitectonically defined human inferior parietal lobule areas reveals similarities to macaques. Neuroimage 58:362-380.

Desikan RS, Ségonne F, Fischl B, Quinn BT, Dickerson BC, Blacker D, Buckner RL, Dale AM, Maguire RP, Hyman BT, Albert MS, Killiany RJ (2006) An automated labeling system for subdividing the human cerebral cortex on MRI scans into gyral based regions of interest. Neuroimage 31:968-980.

Destrieux C, Fischl B, Dale A, Halgren E (2010) Automatic parcellation of human cortical gyri and sulci using standard anatomical nomenclature. Neuroimage 53:1-15.

Felleman DJ, Essen DCV (1991) Distributed hierarchical processing in the primate cerebral cortex. Cereb Cortex 1:1-47.

Fischer E (2011) Visual motion and self-motion processing in the human brain, MPI Series in Biological Cybernetics, Bd. 31: Logos Verlag Berlin GmbH.

Fischl B, Rajendran N, Busa E, Augustinack J, Hinds O, Yeo BTT, Mohlberg H, Amunts K, Zilles K (2008) Cortical folding patterns and predicting cytoarchitecture. Cereb Cortex 18:1973-1980.

Fischl B, van der Kouwe A, Destrieux C, Halgren E, Ségonne F, Salat DH, Busa E, Seidman LJ, Goldstein J, Kennedy D, Caviness V, Makris N, Rosen B, Dale AM (2004) Automatically parcellating the human cerebral cortex. Cereb Cortex 14:11-22.

Fize D, Vanduffel W, Nelissen K, Denys K, Chef d'Hotel C, Faugeras O, Orban GA (2003) The retinotopic organization of primate dorsal V4 and surrounding areas: A functional magnetic resonance imaging study in awake monkeys. J Neurosci 23:7395-7406.

Georgieva S, Peeters R, Kolster H, Todd JT, Orban GA (2009) The processing of three-dimensional shape from disparity in the human brain. J Neurosci 29:727-742.

Glasser MF, Van Essen DC (2011) Mapping human cortical areas in vivo based on myelin content as revealed by T1- and T2-weighted MRI. J Neurosci 31:11597-11616.

Gramfort A, Luessi M, Larson E, Engemann DA, Strohmeier D, Brodbeck C, Parkkonen L, Hämäläinen MS (2014) MNE software for processing MEG and EEG data. NeuroImage 86:446-460.

Gross J, Kujala J, Hämäläinen M, Timmermann L, Schnitzler A, Salmelin R (2001) Dynamic imaging of coherent sources: studying neural interactions in the human brain. Proceedings of the National Academy of Sciences 98:694-699.

Huk AC, Dougherty RF, Heeger DJ (2002) Retinotopy and functional subdivision of human areas MT and MST. J Neurosci 22:7195-7205.

Janssens T, Zhu Q, Popivanov ID, Vanduffel W (2014) Probabilistic and single-subject retinotopic maps reveal the topographic organization of face patches in the macaque cortex. J Neurosci 34:10156-10167.

Kolster H, Peeters R, Orban GA (2010) The retinotopic organization of the human middle temporal area MT/V5 and its cortical neighbors. J Neurosci 30:9801-9820.

Kolster H, Janssens T, Orban GA, Vanduffel W (2014) The retinotopic organization of macaque occipitotemporal cortex anterior to V4 and caudoventral to the middle temporal (MT) cluster. J Neurosci 34:10168-10191.

Krawczyk DC (2002) Contributions of the prefrontal cortex to the neural basis of human decision making. Neurosci Biobehav Rev 26:631-664.

Larsson J, Heeger DJ (2006) Two retinotopic visual areas in human lateral occipital cortex. J Neurosci 26:13128-13142.

Markov NT, Vezoli J, Chameau P, Falchier A, Quilodran R, Huissoud C, Lamy C, Misery P, Giroud P, Ullman S, Barone P, Dehay C, Knoblauch K, Kennedy H (2014) Anatomy of hierarchy: feedforward and feedback pathways in macaque visual cortex. J Comp Neurol 522:225-259.

Moser EI, Kropff E, Moser M-B (2008) Place cells, grid cells, and the brain's spatial representation system. Annu Rev Neurosci 31:69-89.

Nolte G (2003) The magnetic lead field theorem in the quasi-static approximation and its use for magnetoencephalography forward calculation in realistic volume conductors. Physics in medicine and biology 48:3637-3637.

Pandya DN, Seltzer B (1982) Intrinsic connections and architectonics of posterior parietal cortex in the rhesus monkey. J Comp Neurol 204:196-210.

Petrides M, Pandya DN (1999) Dorsolateral prefrontal cortex: comparative cytoarchitectonic analysis in the human and the macaque brain and corticocortical connection patterns. Eur J Neurosci 11:1011-1036.

Reuter M, Schmansky NJ, Rosas HD, Fischl B (2012) Within-subject template estimation for unbiased longitudinal image analysis. Neuroimage 61:1402-1418.

Swisher JD, Halko MA, Merabet LB, McMains SA, Somers DC (2007) Visual topography of human intraparietal sulcus. J Neurosci 27:5326-5337.

Tootell RB, Hadjikhani N, Hall EK, Marrett S, Vanduffel W, Vaughan JT, Dale AM (1998) The retinotopy of visual spatial attention. Neuron 21:1409-1422.

Van Essen DC (2005) Surface-Based Comparisons of Macaque and Human Cortical Organization. In: From Monkey Brain to Human Brain: A Fyssen Foundation Symposium, pp 3-19: Bradford Books.

Van Essen DC, Maunsell JH, Bixby JL (1981) The middle temporal visual area in the macaque: myeloarchitecture, connections, functional properties and topographic organization. J Comp Neurol 199:293-326.

Van Essen DC, Glasser MF, Dierker DL, Harwell J, Coalson T (2012) Parcellations and hemispheric asymmetries of human cerebral cortex analyzed on surface-based atlases. Cereb Cortex 22:2241-2262.

Van Veen BD, van Drongelen W, Yuchtman M, Suzuki A (1997) Localization of brain electrical activity via linearly constrained minimum variance spatial filtering. Biomedical Engineering, IEEE Transactions on 44:867-880.

Vernet M, Quentin R, Chanes L, Mitsumasu A, Valero-Cabré A (2014) Frontal eye field, where art thou? Anatomy, function, and non-invasive manipulation of frontal regions involved in eye movements and associated cognitive operations. Front Integr Neurosci 8:66-66.

Wandell BA, Dumoulin SO, Brewer AA (2007) Visual field maps in human cortex. Neuron 56:366-383.